Int J Adv Manuf Technol (2015) 79:245–254
DOI 10.1007/s00170-015-6838-3

ORIGINAL ARTICLE

Machining tests for identification of location errors on five-axis machine tools with a tilting head

Zhouxiang Jiang · Xiaoqi Tang · Xiangdong Zhou · Shiqi Zheng

Received: 17 July 2014 / Accepted: 20 January 2015 / Published online: 3 February 2015

Abstract Location errors are considered as one of the fundamental errors of five-axis machine tools. For the improvement of machine accuracy, it is important to propose an efficient and accurate identification method of location errors. This paper proposes an identification method of location errors on a five-axis machine tool *with a tilting head* by a set of machining patterns. The machining patterns are proposed under the assumption that the influence of motion errors of each axis on the measuring results is sufficiently small. Location errors of *both linear and rotary axes* can be decoupled and identified. During the measuring of linear axes squareness errors, a new machining method that significantly *increases the moving distances of linear axes* without additional removal of material or enlarged volume of the workpiece is proposed. Also, *a decoupling method* of linear and rotary axes squareness errors relevant to this new machining method is introduced. The measuring accuracy of linear axes squareness errors is greatly improved based on these measuring schemes. The machining tests are performed on a commercial five-axis machine tool with a tilting head. The measurement results are acquired on a coordinate measuring machine, and the identification results are validated by comparing the geometric characteristics of workpieces before and after compensation.

Keywords Five-axis machine tools · Location errors · Machining test · Measurement

Z. Jiang · X. Tang · X. Zhou (✉) · S. Zheng
National NC System Engineering Research Center, Huazhong University of Science & Technology, 1037 Luoyu Road, Wuhan 430074, China
e-mail: xdzhouhust@gmail.com

1 Introduction

1.1 Previous literatures

Five-axis machine tools are extensively used in manufacturing component with complex surfaces, because they have the characteristic of adding two rotary axes to their three-axis configuration. Such machines are more subjected to errors since additional degrees of freedom (DOF) bring additional geometric error sources. For the purpose of improving the motion accuracy of five-axis machines, an efficient and accurate error identification method needs to be excogitated.

The geometric error identification of five-axis machine tools has been widely investigated. Many researchers have studied identification methods relying on various kinds of measuring instruments. The double ball bar (DBB) is applied for identification of geometric errors [1–7]. Lee et al. [1] introduced an approach based on DDB to evaluate offset errors and squareness errors of rotary axes of a five-axis machine tool. Zhang et al. [2] also designed two measuring patterns with DDB to assess rotary axes geometric errors. Calibration methods named R-test and non-contact R-test have also been presented. Bringmann et al. [8–10] and Ibaraki et al. [11–13] have elaborated the usage of R-test in the measurement of both location and component errors of rotary axes. Later, Hong and Ibaraki [14] proposed a non-contact-type R-test with laser displacement sensors as a substitution of the flat-ended probe of R-test, and the performance of the new equipment on location error evaluation has been analyzed.

Some other kinds of automatic error identification process have also been proposed. Ibaraki et al. [15, 16] have demonstrated a new automatic measuring process utilizing the touch-trigger probe. Only single setup is needed for both the touch-trigger probe and the test piece so that the complexity of the

operations is reduced and measuring errors caused by multiple setups are eliminated. Mayer et al. also used touch-trigger probe to identify volumetric distortion [17] and location errors [18] of five-axis machine tools by probing a scale-enriched reconfigurable uncalibrated master ball artifact. In 2010, Ibaraki et al. [19] introduced a method called machining tests to identify rotary axes location errors. In such procedure, a workpiece is machined automatically along predesigned trajectories and then the workpiece geometry parameters are measured on a coordinate measuring machine (CMM).

Compared to the measuring method using DBB and R-test, Ibaraki et al. [19] provides a more intuitive relationship between the machined profiles and error components. Also, the size of the workpiece can be custom according to the size of machine tool. This makes the measuring method more adaptive than DBB and R-test methods constrained by size of equipment.

1.2 Motivations

Even though the previous works mentioned above have great contributions to the measurement of location errors on five-axis machine tools, three important aspects still have not been fully considered.

1. Five-axis machine tools can be classified into three categories depending on the positions where the rotation axes are located. Most literatures and standards [20, 21] about geometric error measurement just focus on the machine configuration with a rotary and tilting table or a universal head. Nevertheless, the configuration with a tilting head has been paid little attention. Only Yang et al. [1] have proposed geometric error identifications by DDB for the configuration with a tilting head.
2. Moreover, few researchers proposed identification methods considering both linear and rotary axes: for DBB method, no identification method for all location errors has been introduced; for R-test, only Bringmann et al. [8] and Mayer et al. [22] proposed measuring methods for link geometric errors of all five axes; for touch-trigger probe, only Mayer [18] estimated ten location errors by probing a scale-enriched reconfigurable uncalibrated master ball artifact. For machining test, no measuring method for all location errors has been proposed.
3. For machining test, the simplest way to measure the three squareness errors of linear axes is to machine two slots long enough with the movement of linear axis to be calibrated. However, the limitation of machine workspace and workpiece volume may make such a machining method an impossible mission with a high cost.

1.3 Contributions

This paper proposes a new machining test scheme to identify 11 location errors of both linear and rotary axes on a five-axis machine tool with a tilting head. The new proposed method addresses the two aspects mentioned in Sect. 1.2.

1. Corresponding machine pattern to each error component is successively proposed and performed on one workpiece. From the measuring results of these machined surfaces on CMM, location errors of *both rotary and linear axes* can be estimated.
2. During the measuring of linear axes squareness errors, a new machining method that significantly increases the moving distances of linear axes without additionally material removal or enlarged volume of the workpiece is proposed. Also, a model-based decoupling method of linear and rotary axes squareness errors relevant to this new machining method is introduced. The measuring accuracy of linear axes squareness errors is greatly improved and the material removal is significantly reduced based on these measuring schemes.

1.4 Structure of the paper

The paper is organized as follows. In Sect. 2, kinematic model including ten location errors of five-axis machine tools with a tilting head is established. In Sect. 3, seven machining patterns and the corresponding algorithm are successively illustrated and formulated. In Sect. 4, geometries of all machined surfaces are probed on a CMM, and the measuring results are represented and used to calculate the location errors. Validations of identified errors are also demonstrated in Sect. 4.

2 Kinematic model including location errors

2.1 Machine configuration

As described in Sect. 1, the machine tool that is concerned in this research is a five-axis machine tool with tilting head and a rotary table as shown in Fig. 1. Linear motions in the *X*-, *Y*-, and *Z*-directions are generated by three linear axes *X*, *Y*, and *Z*, while tilting and rotational motions around the *Y*- and *Z*-directions are generated by two rotary axes *B* and *C*.

2.2 Location errors to be identified

Location errors are defined as general shape and assembly errors of the machine structures which determine the relative locations of motion axes. For the configuration delineated in

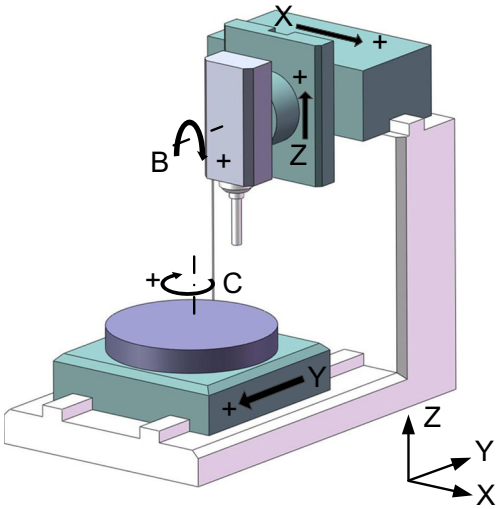

Fig. 1 The configuration of five-axis machine tool considered in this research

Fig. 1, the set of location errors contains 11 elements shown in Table 1. The seven squareness errors and the linear offset of *B*-axis in *X*-direction are inherent errors of the five-axis machine tool. The rest three linear offsets are computer numerical control (CNC) parameter errors which can be directly compensated by revising them in CNC system. Such a set of location errors has been proposed by Ibaraki et al. [15], while Mayer et al. [22] provided another set including eight errors and the CNC parameter errors are omitted.

2.3 Kinematic model of five-axis machine tool with tilting head

The theoretical basis of the error identification approach described in this paper is the kinematic model of machine configuration in Fig. 1. The kinematic model containing location errors is used to calculate the tool center position in the workpiece coordinate system (Fig. 2).

Table 1 Location errors of machine tool configuration in Fig. 1

Symbol	Description
α_{BZ}	Squareness error of *B*-axis around *X*-direction
γ_{BZ}	Squareness error of *B*-axis around *Z*-direction
α_{CY}	Squareness error of *C*-axis around *X*-direction
β_{CY}	Squareness error of *C*-axis around *Y*-direction
δ_{xBZ}	Linear offset of B-axis in X-direction
δ_{zBZ}	Linear offset of *B*-axis in *Z*-direction
δ_{xCY}	Linear offset of *C*-axis in *X*-direction
δ_{yCY}	Linear offset of *C*-axis in *Y*-direction
α_{ZX}	Squareness error of *Z*-axis around *X*-direction
β_{ZX}	Squareness error of *Z*-axis around *Y*-direction
γ_{XY}	Squareness error of *X*-axis around Z-direction

The reference coordinate system is defined as the one attached to the *Y*-axis. The workpiece coordinate system is defined as the one attached to *C*-axis, and its origin is located at the center point of the top surface of rotary table. Then the tool center position in the reference coordinate system is given by

$$^{\mathrm{r}}\boldsymbol{p} = {}^{\mathrm{Y}}\boldsymbol{T}^{\mathrm{X}}\boldsymbol{T}^{\mathrm{Z}}\boldsymbol{T}^{\mathrm{B}}\boldsymbol{p} \tag{1}$$

where

$$\begin{aligned} {}^{B}\boldsymbol{p} &= (-\delta_{xBZ} \quad 0 \quad -\delta_{zBZ}-L \quad 1)^{T} \\ {}^{Z}\boldsymbol{T}_{B} &= \boldsymbol{D}_x(\delta_{xBZ})\boldsymbol{D}_z(\delta_{zBZ})\boldsymbol{D}_a(\alpha_{BZ})\boldsymbol{D}_c(\gamma_{BZ})\boldsymbol{D}_b(B) \\ {}^{X}\boldsymbol{T}_{Z} &= \boldsymbol{D}_b(\beta_{ZX})\boldsymbol{D}_a(\alpha_{ZX})\boldsymbol{D}_x(Z) \\ {}^{Y}\boldsymbol{T}_{X} &= \boldsymbol{D}_z(\gamma_{YX})\boldsymbol{D}_x(X) \end{aligned} \tag{2}$$

The homogeneous transfer matrix (HTM) representing the transformation from the workpiece coordinate system to the reference coordinate system is given by

$$^{r}\boldsymbol{T}_{w} = \boldsymbol{D}_y(Y)\boldsymbol{D}_x(\delta_{xCY})\boldsymbol{D}_y\left(\delta_{yCY}\right)\boldsymbol{D}_b(\beta_{CY})\boldsymbol{D}_a(\alpha_{CY})\boldsymbol{D}_c(-C) \tag{3}$$

Therefore, the tool center position in the workpiece coordinate system can be given by

$$^{\mathrm{w}}\boldsymbol{p} = \left({}^{\mathrm{r}}\boldsymbol{T}\right)^{-1}{}^{\mathrm{r}}\boldsymbol{p} \tag{4}$$

The superscripts (or subscripts) *r*, *w*, *B*, *X*, *Y*, and *Z* represent the machine, workpiece, *B*-, *X*-, *Y*-, and *Z*-axes coordinate system, respectively. ${}^{B}\boldsymbol{p}$ represents the tool center position in the *B*-axis coordinate system. $\boldsymbol{L}$ represents the offset distance from the center point of cutting tool bottom surface to the origin of nominal *B*-axis coordinate system. $\boldsymbol{T}$ represents the HTM describing transformation from the coordinate system of its right-side subscript to the one of its left-side superscript. $\boldsymbol{D}_x(y)$, $\boldsymbol{D}_y(y)$, and $\boldsymbol{D}_z(z)$ represent the HTM for linear motions in *X*-, *Y*-, and *Z*-direction. $\boldsymbol{D}_a(a)$, $\boldsymbol{D}_b(b)$, and $\boldsymbol{D}_c(c)$ represent the HTM for angular motions around X-, Y-, and Z-axes. *X*, *Y*, *Z*, *B*, and *C* represent the command positions of *X*-, *Y*-, *Z*-, *B*-, and *C*-axes, respectively.

3 Machining tests for location errors

According to the uncertainty analysis regarding the influence of motion errors on the measuring results of location errors given by Ibaraki et al. [15], the following machining tests can be proposed under the assumption that the influence of motion errors of each axis on the measuring results is sufficiently small. Before performing the machining procedure, the tilting head and rotary table are regulated to their zero positions. Then a workpiece of hexahedron geometry is roughly fixed on the rotary table as shown in Fig. 3. Sections 3.1–3.6

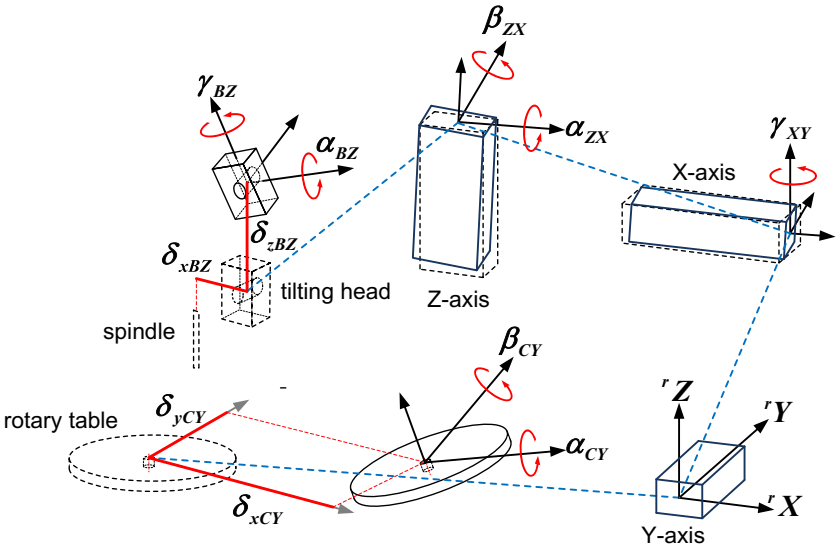

Fig. 2 Kinematic model of five-axis machine considered in this paper

successively represent six machining test patterns for identification of location errors.

3.1 Machining pattern A

This pattern is proposed for the establishment of the *Y*- and *Z*-axes of CMM measuring coordinate. In this pattern, two cutting procedures as shown in Fig. 3 are performed. Each cutting procedure is performed only by the movement of *Y*-axis at the same height.

The *X*-, *Y*-, and *Z*-axis of CMM machine coordinate are, respectively, denoted by ${}^{M}X$, ${}^{M}Y$, and ${}^{M}Z$, while the ones of CMM measuring coordinate are, respectively, denoted by ${}^{m}X$, ${}^{m}Y$, and ${}^{m}Z$. ${}^{m}Y$ can be established by ${}^{M}\gamma_{A}$, which represents the inclination from the side surface of slot *a* to the YOZ plane of CMM measuring coordinate around *Z*-direction as shown in Fig. 4. ${}^{m}Z$ can be established based on ${}^{M}\boldsymbol{n}_{A3}$ which is defined as

$$ {}^{M}\boldsymbol{n}_{A3} = {}^{M}\boldsymbol{n}_{A1} \times {}^{M}\boldsymbol{n}_{A2} \tag{5} $$

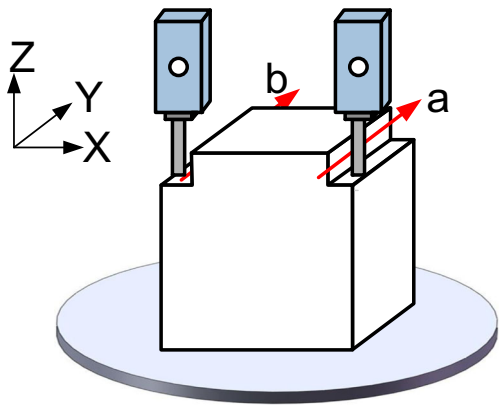

Fig. 3 Machining procedure of pattern A

Where ${}^{M}\boldsymbol{n}_{A1}$ and ${}^{M}\boldsymbol{n}_{A2}$ are measured by probing four non-collinear target points on two bottom surface from $-Z$-directions as shown in Fig. 4.

3.2 Machining pattern B

This pattern is performed to identify two squareness errors of *C*-axis. Four cutting procedure are successively performed at $C=180°$ as shown in Fig. 5. Let ${}^{m}\boldsymbol{n}_{B}(x_B,y_B,z_B,0)^{T}$ denote the normal vector of the bottom surface of machined slot in CMM measuring coordinate. According to the geometrical relationship depicted in Fig. 6 (only identification of β_{CY} is represented, the calculation of α_{CY} is based on the same idea), the squareness errors of rotary axis can be calculated by

$$ \begin{cases} \alpha_{CY} = \arctan(-y_B/z_B)/2 \\ \beta_{CY} = \arctan(x_B/z_B)/2 \end{cases} \tag{6} $$

3.3 Machining pattern C

This pattern is designed for the two linear offsets δ_{xBZ} and δ_{zBZ} of *B*-axis in *X*- and *Z*-direction. δ_{xBZ} is defined as the position

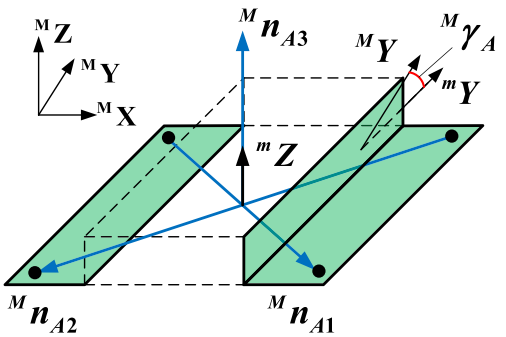

Fig. 4 Establishment of the CMM measuring coordinate

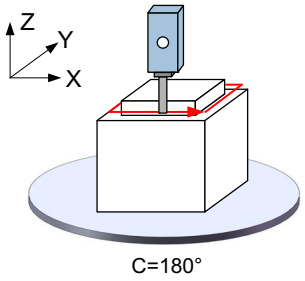

Fig. 5 Machining procedure of pattern B

error in *X*-direction from the actual *B*-axis average line to the spindle axis average line. Generally, δ_{zBZ} is defined as the linear offset in *Z*-direction of *B*-axis average line. For the machine configuration considered in this paper, δ_{zBZ} represents the length error of the tilting head. Three machining procedures are successively performed as shown in Fig. 7. The relationship between δ_{xBZ}, δ_{zBZ} and the measured parameters are represented in Fig. 8. Let ${}^{w}Z_{C1}$, ${}^{w}Z_{C2}$, ${}^{w}Z_{C3}$, respectively, denote the *Z*-axis position command value of steps a, b, and c in the workpiece coordinate. Let ${}^{m}Z_{C1}$, ${}^{m}Z_{C2}$, ${}^{m}Z_{C3}$, respectively, denote the measured height of bottom surface of slots *a*, *b*, and *c*. The actual tool radius denoted by ***R*** can be acquired by measuring the distance between two side surfaces of slot *a*. Then, δ_{xBZ} and δ_{zBZ} can be calculated by

$$\begin{cases} {}^{m}Z_{C3} - {}^{m}Z_{C2} = {}^{w}Z_{C3} - {}^{w}Z_{C2} - 2\delta_{xBZ} \\ {}^{m}Z_{C1} - {}^{m}Z_{C2} = {}^{w}Z_{C1} - {}^{w}Z_{C2} - L + R - \delta_{xBZ} - \delta_{zBZ} \end{cases} \quad (7)$$

3.4 Machining pattern D

In this pattern, a linear offset error of *C*-axis in *Y*-direction is measured. As shown in Fig. 9, first perform a side cutting at *B*=0° and *C*=0°, then rotate *C*-axis by 180° and perform a side cutting again at the same *Y*- and *Z*-position. Let ${}^{w}Y_{D}$ represent the *Y*-position command of steps a and b in the workpiece coordinate. Let ${}^{m}Y_{D1}$ and ${}^{m}Y_{D2}$, respectively, represent the measured *Y*-position of the side surface of steps a and b. As illustrated in Fig. 10, the distance which is supposed to be $|2{}^{w}Y_{D}|$ between two machined surface deviates its nominal value by $2\delta_{yCY}$. Let ***H*** denote the height of machined bottom surface from rotary table in *Z*-direction. Let ***R*** denote the actual tool radius. Considering the influence of α_{BZ} and β_{CY}, then the linear offset of *C*-axis in *Y*-direction is calculated by

$$\delta_{yCY} = \left|{}^{w}Y_{D}\right| - \left|{}^{m}Y_{D1} - {}^{m}Y_{D2}\right|/2 - R + L\sin\alpha_{BZ} + H\sin\beta_{CY} \quad (8)$$

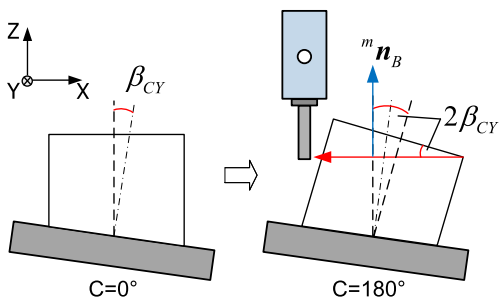

Fig. 6 Identification of β_{CY}

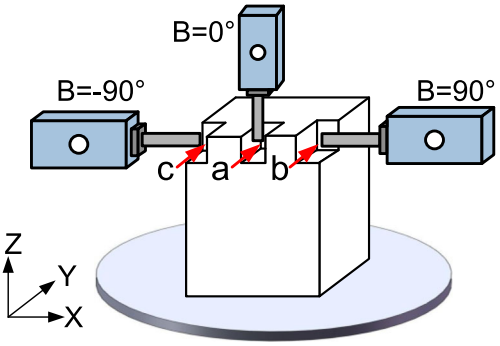

Fig. 7 Machining procedure of pattern C

3.5 Machining pattern E

This pattern is designed for identifying linear offset of *C*-axis average line in *X*-direction. First, perform a side cutting at *B*=0° and *C*=0° as shown in Fig. 11. Then rotate *C*-axis by 180° and perform a side cutting again at the same *X*- and *Z*-positions with the first step. Let ${}^{w}X_{E}$ represent the *X*-position command of steps a and b in the workpiece coordinate. Let ${}^{m}X_{E1}$ and ${}^{m}X_{E2}$, respectively, represent the measured *X*-position of the side surface of steps a and b. As illustrated in Fig. 12, the distance which is supposed to be $|2{}^{w}X_{E}|$ between two machined surface deviates its nominal value by $2\delta_{xCY}$. Let ***H*** denote the height of machined bottom surface from rotary table in *Z*-direction. Let ***R*** denote the actual tool radius.

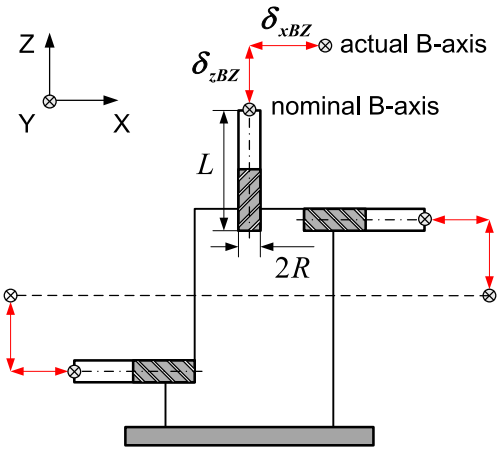

Fig. 8 Identification of δ_{xBZ} and δ_{zBZ}

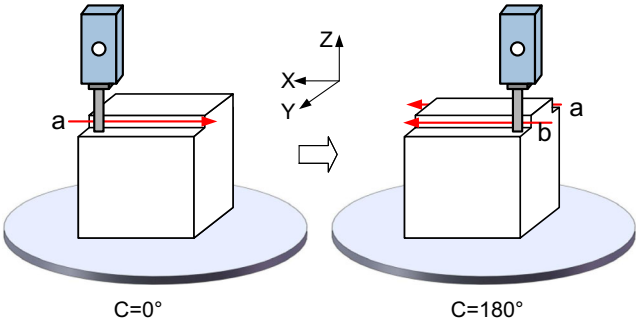

Fig. 9 Machining procedure of pattern D

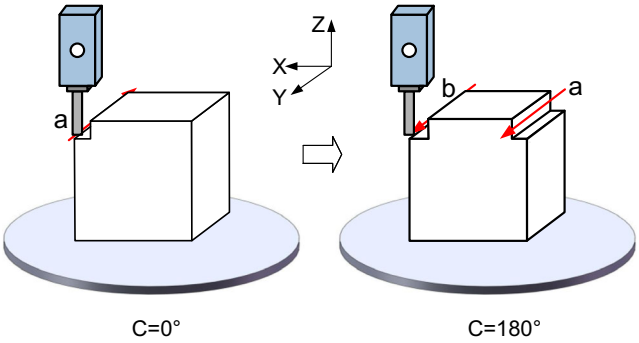

Fig. 11 Machining procedure of pattern E

Considering the influence of β_{CY}, the linear offset between B- and C-axes average lines in X-direction is calculated by

$$\delta_{xCY} = \left|{}^{w}X_E\right| - \left|{}^{m}X_{E1} - {}^{m}X_{E2}\right|/2 - R + H\sin\alpha_{CY} \tag{9}$$

3.6 Machining pattern F

This pattern is designed for the identification of two squareness errors of Z-axis and another squareness error of B-axis around X-direction. Because of the workspace and workpiece volume limitation, it is difficult and costly to rotate B-axis from 0°~180° to measure α_{BZ} and machine a trajectory long enough in X- and Z-direction to measure γ_{XY}, α_{ZX}, and β_{ZX}. Therefore, as shown in Fig. 13, five machining procedures are successively performed at B=0°, ±90°, and ±45°. It has to be mentioned that as shown in Fig. 13, the step a is first performed along $-X$-direction and then $-Y$-direction. Steps b and c are performed along $-Z$-direction. Steps d and e are performed along the direction vertical to the spindle in the XOZ plane.

The side surfaces of steps a and b on the YOZ plane are used to identify the β_{ZX} as shown in Fig. 14. Let ${}^{m}X_{F1}$ and ${}^{m}X_{F2}$, respectively, represent the measured X-position of the YOZ side surfaces of steps a and b. Since the difference of such two side surfaces in X-direction is also influenced by δ_{xBZ} and δ_{zBZ}, the β_{ZX} can be derived by

$${}^{w}X_{F1} - {}^{w}X_{F2} + L - \delta_{xBZ} + \delta_{zBZ} + R + \left({}^{w}Z_{F1} - {}^{w}Z_{F2}\right)\beta_{ZX} = {}^{m}X_{F1} - {}^{m}X_{F2} \tag{10}$$

Then, the XOZ side surfaces of steps a~e are used to identify α_{ZX}, β_{ZX}, γ_{XY}, and α_{BZ}. According to the kinematic model and parameter definition proposed in Sect. 2.3, the center point position of cutting tool bottom surface in machine coordinate can be represented by

$${}^{r}p = \begin{pmatrix} \delta_{xBZ}(1-\cos B) - L\sin B + \delta_{zBZ}(1-\sin B) + X + Z\sin\beta_{ZX} \\ L(\cos B\sin\alpha_{BZ} - \sin B\sin\gamma_{BZ}) + X\sin\gamma_{XY} + Y - Z\sin\alpha_{ZX} \\ \delta_{xBZ}\sin B - (L + \delta_{zBZ})\cos B + Z \\ 1 \end{pmatrix} \tag{11}$$

Let $({}^{w}X_{Fn}, {}^{w}Y_{Fn}, {}^{w}Z_{Fn})(n=1,2,\ldots,5)$ represent the position commands during the machining of XOZ side surfaces of each step in the workpiece coordinate. Let ${}^{m}Y_{Fn}(n=1,2,\ldots,5)$, respectively, represent the measured Y-position of XOZ side surfaces of each step. Based on Eq. (11) and the measured differences in Y-direction among these five XOZ side surfaces and

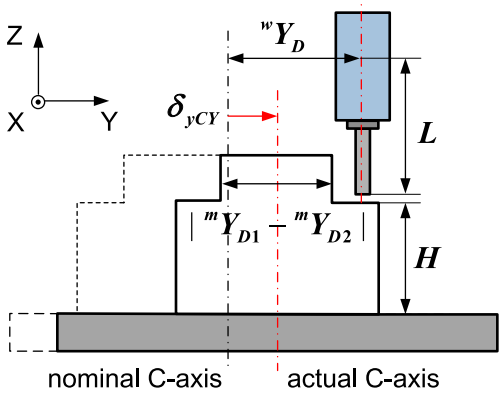

Fig. 10 Identification of γ_{XY} and δ_{yCY}

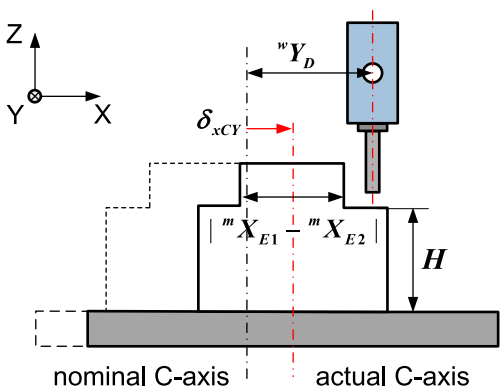

Fig. 12 Identification of δ_{xCY}

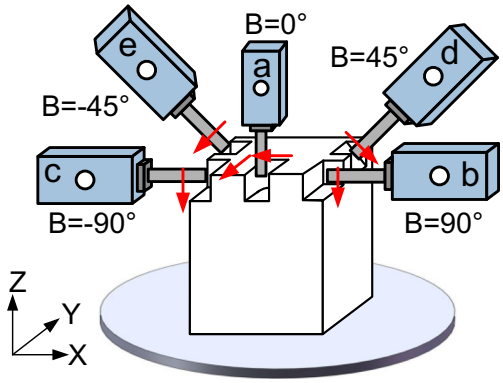

Fig. 13 Machining procedure of pattern F

ignore the high-order terms of small value, four equations of α_{ZX}, β_{ZX}, γ_{XY}, and α_{BZ} can be established as

$$\begin{cases} L\alpha_{BZ} + ({}^{w}X_{F1} - {}^{w}X_{F2})\gamma_{XY} - ({}^{w}Z_{F1} - {}^{w}Z_{F2})\alpha_{ZX} \\ +L\gamma_{BZ} + {}^{w}Y_{F1} - {}^{w}Y_{F2} = {}^{m}Y_{F1} - {}^{m}Y_{F2} \\ L\alpha_{BZ} + ({}^{w}X_{F1} - {}^{w}X_{F3})\gamma_{XY} - ({}^{w}Z_{F1} - {}^{w}Z_{F3})\alpha_{ZX} \\ -L\gamma_{BZ} + {}^{w}Y_{F1} - {}^{w}Y_{F3} = {}^{m}Y_{F1} - {}^{m}Y_{F3} \\ \left(2-\sqrt{2}\right)L\alpha_{BZ}/2 + ({}^{w}X_{F1} - {}^{w}X_{F4})\gamma_{XY} - ({}^{w}Z_{F1} - {}^{w}Z_{F4})\alpha_{ZX} \\ +\sqrt{2}L\gamma_{BZ}/2 + {}^{w}Y_{F1} - {}^{w}Y_{F4} = {}^{m}Y_{F1} - {}^{m}Y_{F4} \\ \left(2-\sqrt{2}\right)L\alpha_{BZ}/2 + ({}^{w}X_{F1} - {}^{w}X_{F5})\gamma_{XY} - ({}^{w}Z_{F1} - {}^{w}Z_{F5})\alpha_{ZX} \\ -\sqrt{2}L\gamma_{BZ}/2 + {}^{w}Y_{F1} - {}^{w}Y_{F5} = {}^{m}Y_{F1} - {}^{m}Y_{F5} \end{cases} \quad (12)$$

The basic idea using simultaneous movement of linear and rotary axes to prolong the linear axes moving distances in this pattern can be expanded to other machine configurations.

4 Experimental analyses

4.1 Experimental setup

The proposed machining test is performed on a commercial middle size five-axis machining tool of the configuration shown in Fig. 1. An aluminum alloy block with the size of 100×100×100 mm is used as the workpiece. The geometric characteristics of machined workpiece are measured on a CMM, *Hexagon global reference*, with measurement uncertainty of $MPE_E(\mu m)=1.0+L/350$.

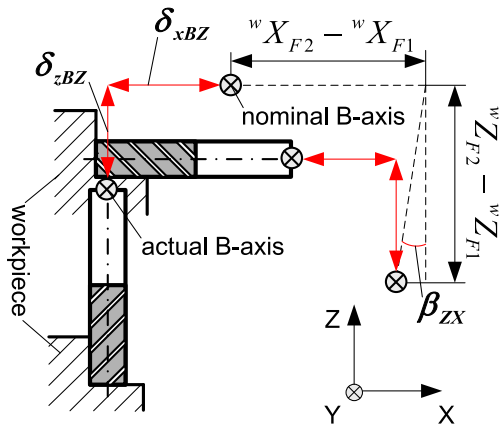

Fig. 14 Identification of β_{ZX}

4.2 Experimental procedure

Machining patterns A–F successively performed on workpiece and machining conditions are provided in Table 2. In Fig. 15, geometrical dimensions of each machining pattern are allowed to be adjusted appropriately for practical situation. Pattern C and the steps a~c of pattern F can be integrated as three slots as shown in Fig. 15a.

4.3 Measurement results and discussion

The profile of machined workpiece on machine tool is shown in Fig. 16. Figures 17, 18, and 19, respectively, represent the measurement results of machining patterns B, D, and E. The measured geometric parameters of all patterns are represented in Table 3. Since measured positions of the target points in patterns C and F are difficult to depict by figures, the measured values of these parameters are represented by the forms of data presentation in Table 3. In Figs. 17, 18, and 19, the probed positions of target points on machined surfaces are depicted by blue dots. The semitransparent planes with green color represent the fitting planes by linear regression from the probed positions of corresponding target points. Location errors of both linear and rotary axes are calculated by Eqs. (6)–(12). The identified location errors are respectively shown in Table 4.

A total of 134 target points are probed during the measurement. Each point is probed by four times and the average position is recorded to minimize the influence of MPE_E of CMM. The distance between each two adjacent points on each machined surface is arranged by 5 mm.

4.4 Validation of measuring results

The measuring results of γ_{XY}, α_{ZX}, and β_{ZX} in machining pattern F are validated by compared with the method proposed by

Table 2 Machining conditions

Cutting tool	CoroMill® Plura solid carbide square shoulder end mill, Φ8 mm, four effective cutting edges
Workpiece material	Aluminum alloy, ASTM5052
Spindle speed	5000 r/min [19]
Feed rate	500 mm/min
Coolant	Water-soluble cutting oil
Cutting depth	0.1 mm for semi-finishing and then finishing at the same path [19]

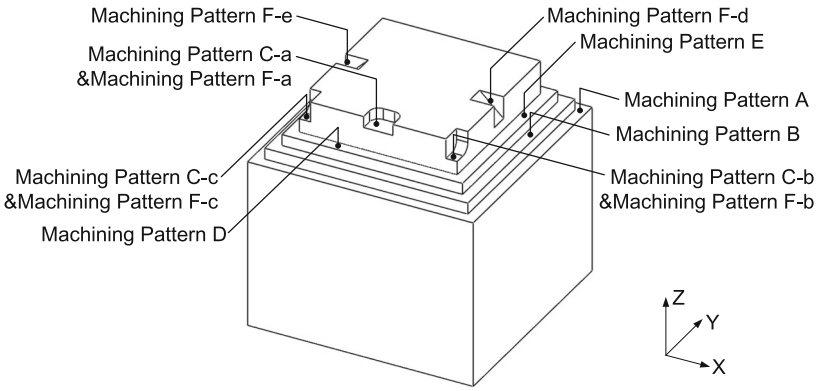

(a) Trimetric view of the workpiece

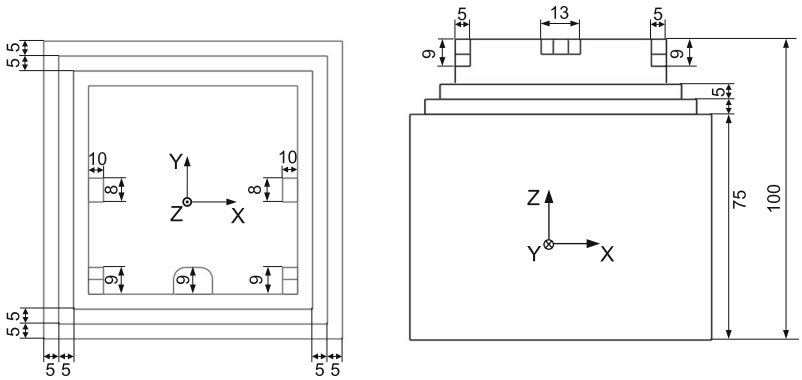

Top view of the workpiece

Front view of the workpiece

(b) Top view and front view of the workpiece

Fig. 15 Geometry of machined workpiece. **a** Trimetric view of the workpiece and **b** top view and front view of the workpiece

Fig. 16 Geometry of the workpiece for identification

Kakino et al. [23] using a double ball bar. Validation results are represented in Table 5 and demonstrate the validity of pattern F proposed in this paper.

The rest of machining patterns in this paper are designed based on intuitive geometric relationships between the location errors and machined trajectories. Also, some of these patterns have already been validated by previous literatures,

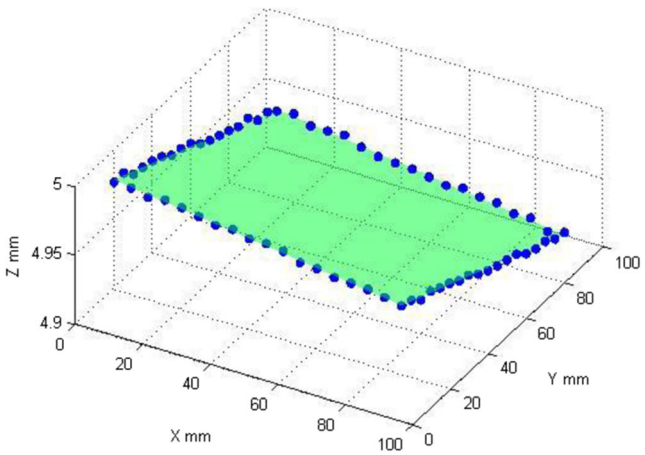

Fig. 17 Measurement results of workpiece surfaces machined by pattern B

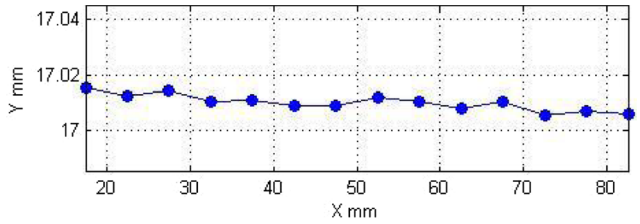

(a) Measured positions of side surface at –Y side

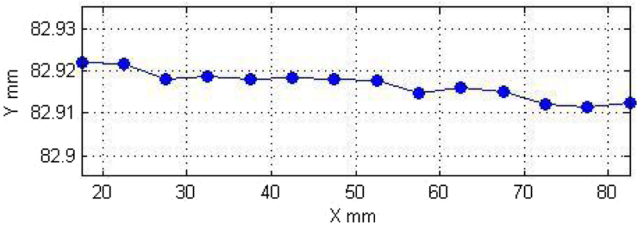

(b) Measured positions of side surface at +Y side

Fig. 18 Measurement results of workpiece surfaces machined by pattern D. **a** Measured positions of side surface at $-Y$ side and **b** measured positions of side surface at $+Y$ side

e.g., patterns D and E are elaborated by Ibaraki et al. [19]. Therefore, the validations of the relative patterns are not emphasized in this section.

5 Conclusions

This paper proposes a machining test to identify 11 location errors of both linear and rotary axes of a five-axis machine tool with a tilting head. During the whole machining process, all the machining patterns are performed on a workpiece. The machined workpiece without complex surfaces is easy to be measured on a CMM. Location errors contained in each measured surface are decoupled and identified. Validation of measuring results is also demonstrated.

This machining test only focuses on location errors of five-axis machine tools. The proposed method is designed under the assumption that the motion errors of linear and rotary axes are sufficiently small and their influence on measuring results is neglectable. However, for higher requirement of location accuracy in the whole workspace of machine tools, motion

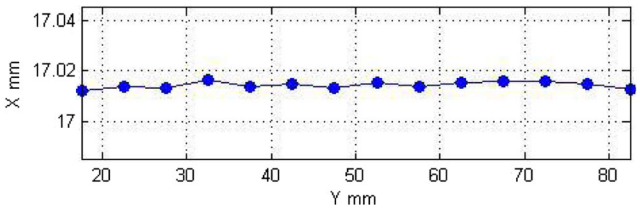

(a) Measured positions of side surface at –X side

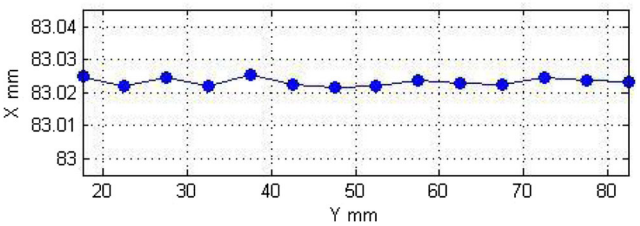

(b) Measured positions of side surface at +X side

Fig. 19 Measurement results of workpiece surfaces machined by pattern E. **a** Measured positions of side surface at $-X$ side and **b** measured positions of side surface at $+X$ side

Table 3 Measured geometric parameters of patterns B–F

Patterns	Parameters	Value
Pattern B	${}^{m}\boldsymbol{n}_{B}$	$(3.496\times10^{-4}, 6.897\times10^{-4}, 1)$
Pattern C	L	218 mm
	R	3.9862 mm
	${}^{w}Z_{C1}, {}^{w}Z_{C2}, {}^{w}Z_{C3}$	95 mm, −137 mm, −137 mm
	${}^{m}Z_{C1}, {}^{m}Z_{C2}, {}^{m}Z_{C3}$	95.0366 mm, 91.1411 mm, 91.1067 mm
Pattern D	${}^{w}Y_{D}$	35 mm
	$\overline{{}^{m}Y_{D1}}, \overline{{}^{m}Y_{D2}}$	17.0101 mm, 82.9169 mm
Pattern E	${}^{w}X_{E}$	35 mm
	$\overline{{}^{m}X_{E1}}, \overline{{}^{m}X_{E2}}$	17.0137 mm, 83.0229 mm
	H	75 mm
Pattern F	${}^{w}X_{F1}, {}^{w}Y_{F1}, {}^{w}Z_{F1}$	(0 mm, 26 mm, 95 mm)
	${}^{w}X_{F2}, {}^{w}Y_{F2}, {}^{w}Z_{F2}$	(263 mm, 26 mm, −133 mm)
	${}^{w}X_{F3}, {}^{w}Y_{F3}, {}^{w}Z_{F3}$	(−263 mm, 26 mm, −133 mm)
	${}^{w}X_{F4}, {}^{w}Y_{F4}, {}^{w}Z_{F4}$	(199 mm, 0 mm, 31 mm)
	${}^{w}X_{F5}, {}^{w}Y_{F5}, {}^{w}Z_{F5}$	(−199 mm, 0 mm, 31 mm)
	${}^{m}Y_{F1}$	15.0158 mm
	${}^{m}Y_{F2}$	15.0543 mm
	${}^{m}Y_{F3}$	15.2947 mm
	${}^{m}Y_{F4}$	14.9593 mm
	${}^{m}Y_{F5}$	15.0093 mm

Table 4 Identified location errors of linear and rotary axes

Error	Identified value
α_{CY}	−0.0198°
β_{CY}	0.01°
δ_{yCY}	0.0317 mm
δ_{xCY}	−0.0195 mm
α_{BZ}	−0.0125°
γ_{BZ}	0.0316°
δ_{xBZ}	−0.0172 mm
δ_{zBZ}	0.0735 mm
α_{ZX}	0.0362°
β_{ZX}	0.0058°
γ_{XY}	−0.0072°

Table 5 Validation of identified location errors of linear axes

Error	Identified value by the new method	Identified value by the traditional method
γ_{XY}	−0.0072°	−0.0105°
α_{ZX}	0.0362°	0.0279°
β_{ZX}	0.0058 mm	0.0083°

errors of each axis are not ignorable. Since machining accuracy of five-axis machine tools is influenced by various kinds of error sources such as motion errors, more attention to machining test for component errors which have not been fully researched will be paid in our future work.

Acknowledgments This research is funded by the National Key Technology R&D Program (Grant NO. 2013ZX04007-021) and Major Project of National Science and Technology (Grant NO. 51475185). The authors also wish to thank Prof. S. Ibaraki for his generous help and instructions.

References

1. Lee KI, Yang SH (2013) Robust measurement method and uncertainty analysis for position-independent geometric errors of a rotary-axis using a double ball-bar. Int J Precis Eng Man 14(2):231–239. doi:10.1007/s12541-013-0032-z
2. Yi Z, Jianguo Y, Kun Z (2013) Geometric error measurement and compensation for the rotary table of five-axis machine tool with double ball bar. Int J Adv Manuf Technol 65:275–281. doi:10.1007/s00170-012-4166-4
3. Abbaszadeh-Mir Y, Mayer JRR, Cloutier G (2002) Theory and simulation for the identification of the link geometric errors for a five-axis machine tool using a telescoping magnetic ball-bar. Int J Prod Res 40(18):4781–4797. doi:10.1080/00207540210164459
4. Zargarbashi SHH, Mayer JRR (2006) Assessment of machine tool trunnion axis motion error, using magnetic double ball bar. Int J Mach Tool&Manuf 46:1823–1834. doi:10.1016/j.ijmachtools.2005.11.010
5. Lee DM, Zankun Z, Lee KI (2011) Identification and measurement of geometric errors for a five-axis machine tool with a tilting head using a double ball-bar. Int J Precis Eng Man 12(2):337–343. doi:10.1007/s12541-011-0044-5
6. Lee KI, Yang S-H (2013) Measurement and verification of position-independent geometric errors of a five-axis machine tool using a double ball-bar. Int J Mach Tool Manuf 70:45–52. doi:10.1016/j.ijmachtools.2013.03.010
7. Tsutsumia M, Tone S, Kato N, Sato R (2013) Enhancement of geometric accuracy of five-axis machining centers based on identification and compensation of geometric deviations. Int J Mach Tool&Manuf 68:11–20. doi:10.1016/j.ijmachtools.2012.12.008
8. Bringmann B, Knapp W (2006) Model-based 'chase-the-ball' calibration of a 5-axes machining center. CIRP Ann-Manuf Technol 55(1):531–534. doi:10.1016/S0007-8506(07)60475-2
9. Bringmann B, Besuchet JP, Rohr L (2008) Systematic evaluation of calibration methods. CIRP Ann-Manuf Technol 57:529–532. doi:10.1016/j.cirp.2008.03.114
10. Bringmann B, Knapp W (2009) Machine tool calibration: geometric test uncertainty depends on machine tool performance. Precis Eng 33:524–529. doi:10.1016/j. precisioneng. 2009. 02. 002
11. Hong CF, Ibaraki S, Matsubara A (2011) Influence of position-dependent geometric errors of rotary axes on a machining test of cone frustum by five-axis machine tools. Precis Eng 35:1–11. doi:10.1016/j.precisioneng.2010.09.004
12. Ibaraki S, Oyama C, Otsubo H (2011) Construction of an error map of rotary axes on a five-axis machining center by static R-test. Int J Mach Tool&Manuf 51:190–200. doi:10.1016/j.ijmachtools.2010.11.011
13. Hong CF, Ibaraki S, Oyama C (2012) Graphical presentation of error motions of rotary axes on a five-axis machine tool by static R-test with separating the influence of squareness errors of linear axes. Int J Mach Tool&Manuf 59:24–33. doi:10.1016/j.ijmachtools.2012.03.004
14. Hong CF, Ibaraki S (2013) Non-contact R-test with laser displacement sensors for error calibration of five-axis machine tools. Precis Eng 37:159–171. doi:10.1016/j.precisioneng.2012.07.012
15. Ibaraki S, Iritani T, Matsushita T (2012) Calibration of location errors of rotary axes on five-axis machine tools by on-the-machine measurement using a touch-trigger probe. Int J Mach Tool&Manuf 58:44–53. doi:10.1016/j.ijmachtools.2012.03.002
16. Ibaraki S, Iritani T, Matsushita T (2013) Error map construction for rotary axes on five-axis machine tools by on-the-machine measurement using a touch-trigger probe. Int J Mach Tool&Manuf 68:21–29. doi:10.1016/j.ijmachtools.2013.01.001
17. Erkan T, Mayer JRR, Dupont Y (2011) Volumetric distortion assessment of a five-axis machine by probing a 3D reconfigurable uncalibrated master ball artifact. Precis Eng 35:116–125. doi:10.1016/j.precisioneng.2010.08.003
18. Mayer JRR (2012) Five-axis machine tool calibration by probing a scale enriched reconfigurable uncalibrated master balls artefact. CIRP Ann-Manuf Technol 61:515–518. doi:10.1016/j.cirp.2012.03.022
19. Ibaraki S, Sawada M, Matsubara A, Matsushita T (2010) Machining tests to identify kinematic errors on five-axis machine tools. Precis Eng 34:387–398. doi:10.1016/j.precisioneng.2009.09.007
20. NAS 979: uniform cutting test, NAS series, metal cutting equipment specifications. 1969:34–7
21. ISO 10791 series, Test conditions for machining centres, International Organization for Standardization; 1998
22. Zargarbashi SHH, Mayer JRR (2009) Single setup estimation of a five-axis machine tool eight link errors by programmed end point constraint and on the fly measurement with Capball sensor. Int J Mach Tool&Manuf 49:75–766. doi:10.1016/j.ijmachtools.2009.05.001
23. Kakino Y, Ihara Y, Shinohara A (1993) Accuracy inspection of NC machine tools by double ball bar method. Hanser Publishers